



***Ab initio* determination of the magnetic ground state of pyrochlore $Y_2Mn_2O_7$** Mohammad Amirabbasi and Mojtaba Alaei ^{*}*Department of Physics, Isfahan University of Technology, Isfahan 84156-83111, Iran* (Received 14 May 2020; revised 18 July 2020; accepted 17 August 2020; published 3 September 2020)

There are two discrepant experimental results on the magnetic ground state of $Y_2Mn_2O_7$; one study proposes a spin-glass state, while the other introduces the material as a ferromagnet. In this study, we attempt to resolve this issue by employing density functional theory and Monte Carlo simulations. We derive different spin models by varying the Hubbard U parameter in *ab initio* GGA+ U calculations. For most of the range of Hubbard U , we find that the leading terms in the spin Hamiltonian are biquadratic and nearest-neighbor Heisenberg exchange interactions. By comparing Monte Carlo simulations of these models with the experiments, we find a ferromagnetic ground state for $Y_2Mn_2O_7$ to be the most compatible with experiments. We also consider $Y_2Mo_2O_7$ as a prototype of the defect-free pyrochlore system with spin-glass behavior and compare it with $Y_2Mn_2O_7$. The orbital degrees of freedom are considered as a leading factor in converting a defect-free pyrochlore such as $Y_2Mn_2O_7$ to a spin-glass system. By changing the d orbital occupations of Mo atoms, our GGA+ U calculations for $Y_2Mo_2O_7$ indicate many nearly degenerate states with different d orbital orientations, which reveals d orbital degrees of freedom in this material. However, for $Y_2Mn_2O_7$, we find a single ground state with a fixed orbital orientation. Consequently, all of our *ab initio* approaches confirm $Y_2Mn_2O_7$ is a ferromagnetic system.

DOI: [10.1103/PhysRevB.102.125105](https://doi.org/10.1103/PhysRevB.102.125105)**I. INTRODUCTION**

The geometrical frustration [1] of magnetic pyrochlore oxides, with the chemical formula $A_2B_2O_7$ [2,3], is generating more research on these materials. The geometrical frustration is due to the networks of corner-sharing tetrahedrons (Fig. 1 indicates one of these networks), which are formed by the magnetic ions residing on A and B sites. Due to the diverse nature of magnetic ions, their interactions, and geometrical frustration, the ground state can be spin ice [4,5], spin liquid [6], or spin glass [7]. If this frustration accompanies randomness such as chemical disorders and crystallographic defects, magnetic moments of ions will freeze with random spatial orientations [8,9], creating a spin-glass phase. Unconventional spin-glass behavior for some pyrochlore oxides such as $Y_2Mo_2O_7$ [10–14], $Y_2Mn_2O_7$ [15], $Tb_2Mo_2O_7$ [16], and $A_2Sb_2O_7$ ($A=Mn, Co, Ni$) [17] has been observed despite the fact that their crystal structures are highly pure and chemically ordered. One of the most exciting pyrochlore spin glasses is $Y_2Mo_2O_7$, in which, instead of chemical disorder, the orbital degrees of freedom play a role in converting the material to a spin-glass system. While, for $Y_2Mo_2O_7$, theoretical and experimental evidence of its spin-glass behavior is available, for $Y_2Mn_2O_7$, a very similar compound, the experimental results are inconsistent, and there is no theoretical study of its low-temperature magnetic ground state.

Reimers *et al.* showed [15] that $Y_2Mn_2O_7$ exhibits experimental evidence of the spin-glass state below critical temperature ($T_c = 20$ K), such as splitting of

zero-field cooling and field-cooling dc susceptibility, the frequency-dependent ac susceptibility cusp, a broad maximum peak in the magnetic specific heat near T_c , and no magnetization saturation in the presence of magnetic field even at low temperatures. Also, neutron scattering measurements revealed that there is no Bragg magnetic peak below T_c . In contrast, Shimakawa *et al.* observed [18] that there is a λ peak at $T_c = 16$ K of the magnetic specific heat, a signature of the long-range ferromagnetic ground state similar to other members of this oxide family ($In_2Mn_2O_7$, $Lu_2Mn_2O_7$, $Tl_2Mn_2O_7$). In both studies, the authors claim that samples of $Y_2Mn_2O_7$ are highly pure and free of chemical disorders.

The motivation of the present study is to resolve the issue of the low-temperature magnetic ground state of $Y_2Mn_2O_7$ by means of the density functional theory (DFT) and classical Monte Carlo (MC) simulations. We derive an effective spin Hamiltonian for $Y_2Mn_2O_7$. The Hamiltonian consists of Heisenberg exchange, biquadratic (B), and Dzyaloshinskii-Moriya (DM) interactions and single-ion anisotropy Δ . Using this Hamiltonian, the critical and Curie-Weiss temperatures, as well as magnetic order, are investigated using Monte Carlo simulations. Our calculations show that $Y_2Mn_2O_7$ is a pyrochlore ferromagnet. To ensure that the ground state is a ferromagnet, not a spin glass, we investigate d -orbital degrees of freedom as one of the possible sources of spin glass. Since $Y_2Mo_2O_7$ is a spin glass (due to d -orbital degrees of freedom), we also study this material as a prototype of unconventional spin glass for comparison. Our *ab initio* results indicate d orbital degeneracy (orbital degrees of freedom) for Mo in $Y_2Mo_2O_7$, while the Mn d state is free of orbital degeneracy in $Y_2Mn_2O_7$.

^{*}m.alaei@iut.ac.ir

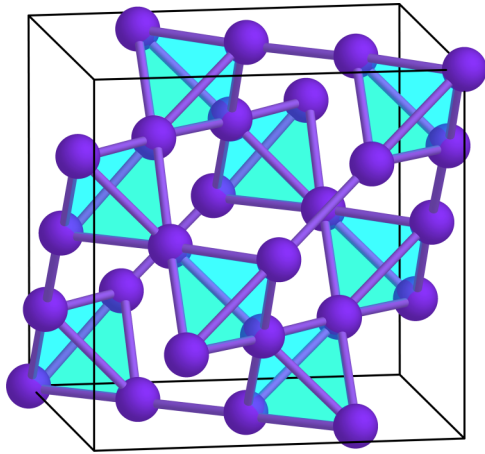


FIG. 1. The corner-sharing tetrahedral network of the Mn (Mo) atom in the cubic pyrochlore $Y_2Mn_2O_7$ ($Y_2Mo_2O_7$).

In the following sections, we explain why $Y_2Mn_2O_7$ is a pyrochlore ferromagnet, not a spin glass. In Sec. II, we present the details of the DFT and Monte Carlo computations. Section III is devoted to the spin Hamiltonian and critical properties of $Y_2Mn_2O_7$. Furthermore, we compare $Y_2Mn_2O_7$ with $Y_2Mo_2O_7$ in terms of orbital degeneracy for the minority-spin state. Finally, in Sec. IV a summary is given.

II. COMPUTATIONAL DETAILS

For all of the *ab initio* calculations, we adopt experimental parameters for both $Y_2Mn_2O_7$ and $Y_2Mo_2O_7$. These pyrochlores crystallize in a cubic structure with the $Fd\bar{3}m$ space group. Both Mn (Mo) and Y ions form separate corner-sharing tetrahedral networks (Fig. 1 shows tetrahedral networks of Mn atoms in the pyrochlore structure), where Y, Mn (Mo), O(1), and O(2) atoms occupy $16d$, $16c$, $48f$, and $8a$ Wyckoff positions, respectively. From x-ray powder diffraction, the x -positional internal parameter and lattice constant of $Y_2Mn_2O_7$ are determined to be 0.3274(8) and 9.901 Å, respectively [19]. For $Y_2Mo_2O_7$, powder neutron diffraction identifies the internal parameter as 0.3382(1) and the lattice constant as 10.230(1) Å [20].

In this work, we use the FLEUR [21] and QUANTUM ESPRESSO [22] (QE) codes for *ab initio* calculations. The former operates based on the full-potential linearized augmented plane wave (FPLAPW), while the latter uses the plane-wave pseudopotential approach. For FPLAPW calculations, the optimized cutoff of wave function expansion in the interstitial region is set to $k_{\max} = 4.2$ a.u.⁻¹. The muffin-tin radii of Y, Mn, and O atoms are set to 2.6, 2.1, and 1.4 a.u., respectively. For all QE calculations, the optimized 40- and 400-Ry cutoffs have been considered for expanding wave function and charge density in the plane wave, respectively. In QE calculations, we approximate electron-ion interactions using the GBRV ultrasoft pseudopotential [23]. For the exchange-correlation energy, we employ the Perdew-Burke-Ernzerhof parametrization of the generalized gradient approximation (GGA) [24]. For the Bader charge analysis, we use CRITIC2 [25,26] with QE.

We use the GGA+ U approximation to correct the on-site Coulomb interaction for 3d and 4d electrons of Mn and Mo atoms, respectively. The implementation of GGA+ U in FLEUR follows Liechtenstein's approach. The approach needs two parameters, U (on-site Coulomb repulsion) and J_H (the on-site Hund's exchange). However, in our QE calculations, we use Dudarev's approach, which needs only effective on-site Coulomb repulsion ($U_{\text{eff}} = U - J_H$). Because for many oxides $J_H \sim 1$ eV [27,28], we use this value for J_H in all FPLAPW calculations. To have an estimation of the U_{eff} parameter, we employ the linear-response calculation method implemented in QE [29]. For this estimation, we use the conventional cell of $Y_2Mn_2O_7$ (containing 88 atoms). We also estimate U_{eff} through a more exact procedure called a self-consistent Hubbard U [30]. The method calculates U_{eff} using the repeating linear-response calculation within GGA+ U until U_{eff} reaches a convergent value.

We derive the spin model Hamiltonian for $Y_2Mn_2O_7$ from FPLAPW total energies of different magnetic configurations. In order to capture the physics of exchange interactions and critical properties of the $Y_2Mn_2O_7$ pyrochlore, we define the spin Hamiltonian as follows:

$$H = -\frac{1}{2} \sum_{i \neq j} J_{ij} (\vec{S}_i \cdot \vec{S}_j) + \frac{1}{2} B \sum_{\text{n.n.}} (\vec{S}_i \cdot \vec{S}_j)^2 + \frac{1}{2} D \sum_{\text{n.n.}} \hat{D}_{ij} \cdot (\vec{S}_i \times \vec{S}_j) + \Delta \sum_i (\vec{S}_i \cdot \vec{d}_i)^2, \quad (1)$$

where \vec{S}_i denotes the unit vector of the magnetic moment at the i th lattice site, J_{ij} are the Heisenberg exchange parameters up to the third neighbor (J_1, J_2, J_{3a}) (see Ref. [31] for more details), B is the biquadratic exchange interaction between the nearest neighbors, D shows the strengths of the DM interaction, and Δ is the strength of single-ion anisotropy. Also, \hat{D}_{ij} shows the direction of DM vectors which is determined by Moriya rules [32], and the vector \vec{d}_i is the single-ion easy-axis direction at the i th site. In our previous study [31], we demonstrated that Eq. (1) enables us to describe the magnetic properties of the pyrochlore FeF_3 . The similarity between the structures of pyrochlores FeF_3 and $Y_2Mn_2O_7$ makes Eq. (1) suitable for $Y_2Mn_2O_7$ too. The similarity comes from the facts that (i) the structures of both $Y_2Mn_2O_7$ and FeF_3 have the same space group ($Fd\bar{3}m$), (ii) Mn and O(1) in $Y_2Mn_2O_7$ have the same Wyckoff positions as Fe and F in FeF_3 , and (iii) O(1) is intermediate between Mn atoms in $Y_2Mn_2O_7$ and F is intermediate between Fe atoms in FeF_3 .

The calculation of different spin Hamiltonian terms is divided into two categories. The first category is related to the Heisenberg term up to the third-nearest neighbor. To this end, we use the conventional unit cell (88 atoms) with a $4 \times 4 \times 4$ Monkhorst-Pack k -point mesh. The second category is devoted to other spin Hamiltonian terms. Since the nearest neighbor is important for these terms, we consider the primitive cell (22 atoms) with a $6 \times 6 \times 6$ Monkhorst-Pack k -point mesh. To derive Heisenberg coupling constants, we calculate the GGA+ U total energies of several collinear magnetic configurations. Then through the least-squares method, we obtain the Heisenberg constants (J_1, J_2, J_{3a}) by fitting the Heisenberg part of the spin Hamiltonian to the GGA+ U total energies.

TABLE I. Calculated spin Hamiltonian constants for different U_{eff} parameters. Negative and positive values for Heisenberg exchanges parameters denote antiferromagnetic and ferromagnetic exchange interactions, respectively. The values of critical and Curie-Weiss temperatures for different U_{eff} parameters were calculated with the Monte Carlo simulation.

U_{eff} (eV)	J_1 (meV)	J_2 (meV)	J_{3a} (meV)	B (meV)	D (meV)	Δ (meV)	T_C (K)	Θ_{CW} (K)
2.36	-0.69	-0.14	-0.28	-0.79	0.13	-0.12	7.0	-30.4
3.36	-0.02	-0.10	-0.17	-0.84	0.13	-0.12	7.4	-8.6
4.36	0.60	-0.07	-0.08	-0.89	0.13	-0.12	8.3	8.6
4.83	0.89	-0.06	-0.05	-0.92	0.13	-0.12	13.7	16.5
5.36	1.22	-0.04	-0.01	-0.96	0.14	-0.12	21.1	25.5
Expt.							20 [15], 16 [18]	41 [15], 50 [18]

For biquadratic interaction B , we calculate the GGA+ U total energies of several noncollinear magnetic configurations with a zero magnetic summation at each Mn tetrahedron. It can easily be demonstrated that for such magnetic arrangements, the Heisenberg term is degenerate. Therefore, the GGA+ U total energy differences of these magnetic configurations are related to nonrelativistic interactions such as the biquadratic interaction. To obtain D and Δ , we include spin-orbit coupling (SOC) in the total energy calculations (GGA+ U +SOC). Then by computing the total energies of some noncollinear magnetic configurations which are degenerate with respect to the biquadratic and Heisenberg parts of the spin Hamiltonian, we extract D and Δ . The details of these calculations were reported in Ref. [31].

To explore the low-temperature magnetic ground state and critical properties of $\text{Y}_2\text{Mn}_2\text{O}_7$, we perform Monte Carlo simulations using the replica exchange method [33] as implemented in the Esfahan Spin Simulation package (ESpinS) [34]. We use three-dimensional lattices consisting of $N \times L^3$ spins, where $L = 11$ is the linear size of the simulation cell and N is the number of spins ($N = 4$ for one tetrahedron); 10^6 Monte Carlo steps (MCs) per spin at each temperature are considered for the thermal equilibrium and data collection, respectively. To reduce the correlation between the successive data, the interval between measurements is set to 10 MCs.

III. RESULTS AND DISCUSSION

A. Spin Hamiltonian of $\text{Y}_2\text{Mn}_2\text{O}_7$

Table I summarizes calculated H terms for different U_{eff} parameters as well as T_C and Θ_{CW} , which were obtained by means of MC simulations of Eq. (1). From the linear response and self-consistent linear-response approach, we obtain $U_{\text{eff}} = 4.36$ eV and 4.83 eV, respectively. According to Table I, for these U_{eff} values, the type of nearest-neighbor exchange interaction is ferromagnetic. The linear-response method provides a rough estimation of U_{eff} , which allows us to tune U_{eff} around this estimation to obtain more consistent results with the experiment. Therefore, we also consider $U_{\text{eff}} = 3.36$ eV and $U_{\text{eff}} = 5.36$ eV. Because at $U_{\text{eff}} = 3.36$ eV, J_1 is approximately zero, we also add $U_{\text{eff}} = 2.36$ eV in our Hubbard parameter list, where we guess J_1 becomes antiferromagnetic.

According to Table I, the most influential interactions are the first nearest-neighbor Heisenberg and biquadratic exchange. For the Heisenberg exchange J_1 , there is a transition at $U_{\text{eff}} = 3.36$ from antiferromagnetic (negative J_1) to ferromag-

netic (positive J_1) type. The anisotropic exchange interactions (D and Δ), unlike isotropic terms (J_1 and B), have no changes with U_{eff} . The positive D (direct Dzyaloshinskii-Moriya interaction) tends to choose noncollinear spin orientations [35,36] (all-in/all-out phase), but this interaction is weaker compared to other interactions, and the ground state is likely to be less dependent on this interaction. In contrast, the biquadratic interaction B becomes slightly stronger with increasing U_{eff} , and its negative value indicates that magnetic moments tend to choose collinear spin orientation.

B. Monte Carlo simulations

For each U_{eff} , the corresponding spin model Hamiltonian is used in MC simulations. From MC simulations, we obtain thermodynamic magnetic properties of $\text{Y}_2\text{Mn}_2\text{O}_7$, such as critical (T_C) and Curie-Weiss (Θ_{CW}) temperatures. To extract Θ_{CW} , we linearly extrapolate the reverse magnetic susceptibility data at high temperature (250–300 K) to the low temperature, as shown in Fig. 2(b). For estimation of T_C , we use the peak of the magnetic specific heat [Fig. 2(a)]. Comparing T_C and Θ_{CW} with experiment (Table I) reveals that the MC results related to self-consistent U_{eff} (i.e., 4.83 eV) and also $U_{\text{eff}} = 5.36$ eV are comparable to experimental data. Also, according to Table I, there is a transition from antiferromagnetism ($\Theta_{\text{CW}} < 0$) to ferromagnetism ($\Theta_{\text{CW}} > 0$) when U_{eff} changes from 3.36 to 4.36. So although we find $U_{\text{eff}} = 5.36$ eV to be the best of our GGA+ U results, considering the two extrema of our results, i.e., $U_{\text{eff}} = 2.36$ eV (antiferromagnetic phase) and $U_{\text{eff}} = 5.36$ eV (ferromagnetic phase), can be instructive.

For $U_{\text{eff}} = 5.36$ eV, ferromagnetic J_1 dominates over other interactions, and it is expected to have a ferromagnetic phase. The strong negative biquadratic interaction ($B = -0.96$ meV) prevents noncollinear magnetism, which can be caused by single-ion ($\Delta = -0.12$ meV) and Dzyaloshinskii-Moriya ($D = 0.14$ meV) interactions. However, for $U_{\text{eff}} = 2.36$ eV, although J_1 and B play a significant role, the third-nearest-neighbor exchange interaction J_{3a} also contributes to determining the magnetic ordering configuration at low temperatures. In the following, we consider the effect of J_{3a} on the magnetic ordering of the system.

To have a correct sense of magnetic ordering below the transition temperature for the $U_{\text{eff}} = 2.36$ case, we take a snapshot of the magnetic configuration at 0.5 K (see Fig. 3). From the snapshot, we can easily recognize a collinear antiferromagnetic arrangement in most of the tetrahedrons. However, in few of the tetrahedrons, the magnetic arrangement

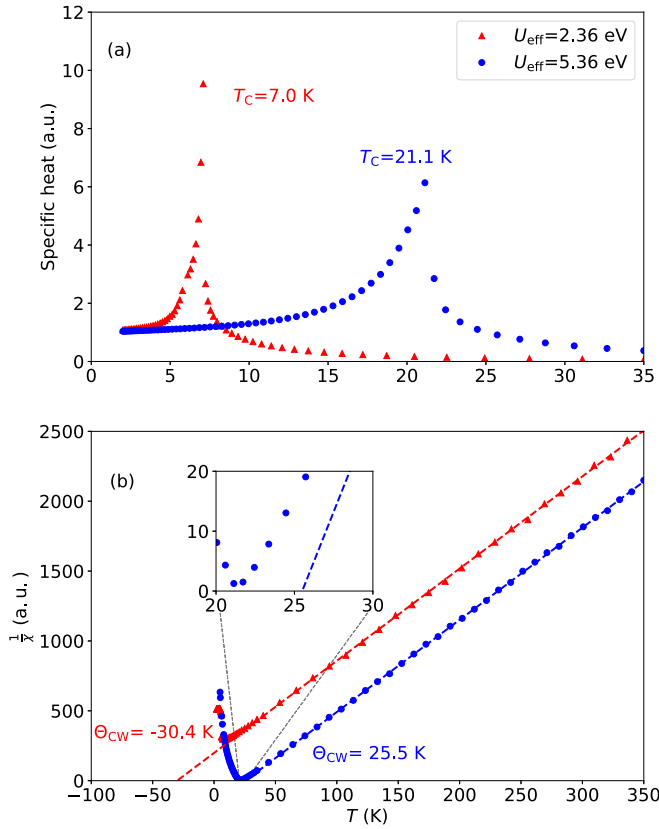


FIG. 2. Monte Carlo simulation results using a lattice of linear size $L = 11$: (a) Magnetic specific heat and (b) reverse magnetic susceptibility for $U_{\text{eff}} = 2.36$ and 5.36 eV. Dashed lines are fitting lines to data in the range 250–300 K. The inset zoom shows reverse magnetic susceptibility in the 20–30 K interval for $U = 5.36$ eV.

does not follow a perfect antiferromagnetic configuration (i.e., $|\mathbf{S}_1 + \mathbf{S}_2 + \mathbf{S}_3 + \mathbf{S}_4| \approx 0$, where $\mathbf{S}_1 \cdots \mathbf{S}_4$ indicate the unit vectors of the spin directions at each vertex). Still, the characteristic feature in all of the tetrahedrons is that magnetic moments are approximately collinear. Therefore, to consider the magnetic ordering, we guess absolute total magnetization, $|\mathbf{S}_1 + \mathbf{S}_2 + \mathbf{S}_3 + \mathbf{S}_4|$, is a proper measurement for magnetic order inside tetrahedrons (for a collinear arrangement, $|\mathbf{S}_1 + \mathbf{S}_2 + \mathbf{S}_3 + \mathbf{S}_4|$ can be 4, 2, or 0). The probability densities of

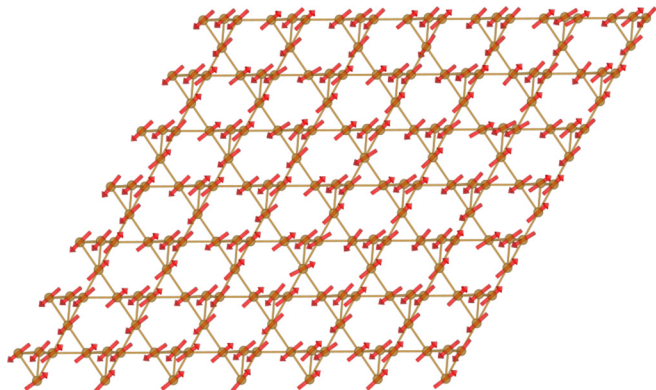


FIG. 3. A two-dimensional slice ($7 \times 7 \times 1$) of a spin snapshot at $T = 0.5$ K for $U_{\text{eff}} = 2.36$ eV.

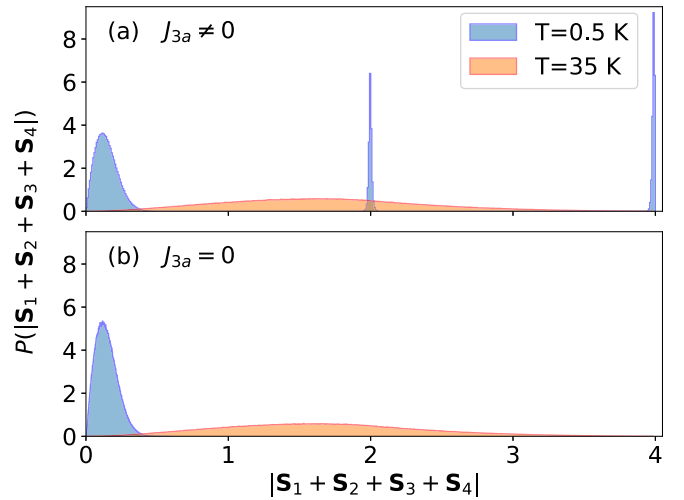


FIG. 4. The probability distribution of $|\mathbf{S}_1 + \mathbf{S}_2 + \mathbf{S}_3 + \mathbf{S}_4|$ inside tetrahedrons at $T = 0.5$ K for $U_{\text{eff}} = 2.36$ eV (a) with J_{3a} and (b) without J_{3a} .

$|\mathbf{S}_1 + \mathbf{S}_2 + \mathbf{S}_3 + \mathbf{S}_4|$ at $T = 0.5$ K (below the transition temperature) and $T = 35$ K (above the transition temperature) are represented in Fig. 4(a). The distribution of $|\mathbf{S}_1 + \mathbf{S}_2 + \mathbf{S}_3 + \mathbf{S}_4|$ indicates the collinear magnetism (the peaks are around 0, 2, and 4), but in many tetrahedrons, a perfect antiferromagnetic arrangement is disturbed. However, an almost perfect antiferromagnetic arrangement will appear [Fig. 4(b)] if we switch off the third-nearest-neighbor exchange interaction J_{3a} . Therefore, although our MC simulation shows J_{3a} has a very small effect on transition temperature, it completely changes the magnetic order.

C. Orbital degree of freedom in $\text{Y}_2\text{Mn}_2\text{O}_7$ and $\text{Y}_2\text{Mo}_2\text{O}_7$

Our *ab initio* calculations show that for calculated U_{eff} using both linear response (4.36 eV) and self-consistent linear response (4.83 eV), the low-temperature magnetic ground state has a ferromagnetic order. Also, MC simulations confirm the compatibility of the derived spin Hamiltonian from GGA+ U at $U_{\text{eff}} = 4.83$ and 5.36 eV with the experimental thermodynamic quantities, T_C and Θ_{CW} . However, some experimental evidence indicates spin-glass behavior for this compound [15]. Since experimental results for $\text{Y}_2\text{Mn}_2\text{O}_7$ confirm no chemical disorder is present in this system, we suggest that $\text{Y}_2\text{Mn}_2\text{O}_7$ may have an orbital degree of freedom mechanism similar to $\text{Y}_2\text{Mo}_2\text{O}_7$, which leads them to a spin-glass behavior [10,37]. In the following, we compare $\text{Y}_2\text{Mn}_2\text{O}_7$ and $\text{Y}_2\text{Mo}_2\text{O}_7$ to confirm firmly that $\text{Y}_2\text{Mn}_2\text{O}_7$ cannot be a spin glass similar to $\text{Y}_2\text{Mo}_2\text{O}_7$.

1. Electronic structure differences between $\text{Y}_2\text{Mn}_2\text{O}_7$ and $\text{Y}_2\text{Mo}_2\text{O}_7$ at the GGA level

In the literature of magnetic pyrochlore oxides [3], the valence state for pyrochlore oxides is simplified as $A_2^{+3}B_2^{+4}O_7^{-2}$. This simplification leads to $3d^3$ - and $4d^2$ -electron configurations in d orbitals for $\text{Y}_2\text{Mn}_2\text{O}_7$ and $\text{Y}_2\text{Mo}_2\text{O}_7$, respectively [15,37]. However, using the Bader charge analysis, we estimate the valence state within the GGA

TABLE II. Charge distribution among Mn d and Mo d orbitals in $Y_2Mn_2O_7$ and $Y_2Mo_2O_7$, respectively, obtained by GGA Lowdin charge analysis.

Atom	Spin	d_{tot}	$(d_{z^2}, d_{x^2-y^2})$	(d_{xy}, d_{xz}, d_{yz})
Mn	↑	3.9589	0.9450	0.6897
	↓	1.1277	0.1819	0.2546
Mo	↑	3.0019	0.6326	0.5789
	↓	1.1764	0.1923	0.2639

calculations as follows: $Y_2^{+2.18}Mn_2^{+1.89}O(1)_5^{-1.12}O(2)_2^{-1.39}$ and $Y_2^{+2.20}Mo_2^{+2.19}O(1)_5^{-1.23}O(2)_2^{-1.40}$. Lowdin charge analysis also confirms these results. In addition, Lowdin charge analysis indicates how electrons distribute among d orbitals (Table II). Due to the hybridization of the d orbitals of Mn (Mo) with p orbitals of oxygen atoms, the occupation of d orbitals of Mn (Mo) is fractional. The spin-minority occupation for both Mn and Mo is about 1 electron, while the spin-majority occupation is about 4 and 3 for Mn and Mo, respectively. To have a better comparison, we also compare the density of states (DOS) of d Mo and d Mn states at the GGA level of DFT theory (Fig. 5). According to Fig. 5, $Y_2Mn_2O_7$ is an insulator, indicating that band theory gives at least a correct state (i.e., insulating) for this material. However, DOS of $Y_2Mo_2O_7$ shows some d states at the Fermi level despite the fact that $Y_2Mo_2O_7$ is a semiconductor [38]. The reason for such a difference is that while crystal field

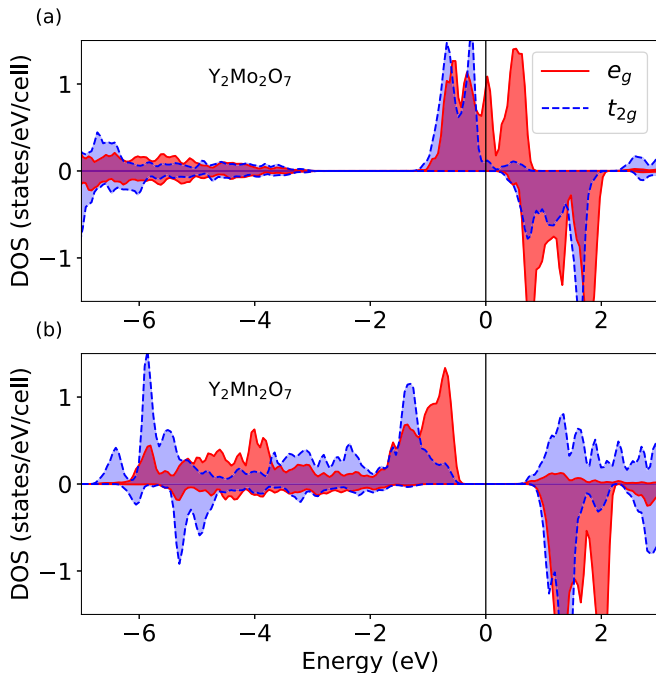


FIG. 5. Density of state (DOS) of (a) the Mo d orbital in $Y_2Mo_2O_7$ and (b) the Mn d orbital in $Y_2Mn_2O_7$. The positive and negative DOSs indicate majority-spin and minority-spin states, respectively. The magnetic moments of Mn and Mo (obtained by subtracting the spin-majority population from the spin-minority population) are $2.83\mu_B$ and $1.83\mu_B$, respectively. For these calculations, we choose the ferromagnetic arrangement and use spin-polarized GGA.

splitting helps the $3d^5$ configuration of $Y_2Mn_2O_7$ become an insulator, the lack of crystal field splitting at the Fermi level leads the $4d^4$ configuration of $Y_2Mo_2O_7$ to the metal in GGA calculations.

2. Orbital degree of freedom

The GGA+ U calculations are generally based on the density matrix of atomic orbital states such as d states. In some systems, there are several choices for density-matrix occupations, and therefore, there are several electronic structures for the system [39,40] (more precisely, GGA+ U faces the multim minima problem). In practice, the correct density-matrix occupation can be chosen by comparing the GGA+ U total energies. Principally, for systems such as $Y_2Mn_2O_7$ in which GGA predicts correctly the system is an insulator, there is a unique density-matrix occupation (i.e., a single minimum), and there is no need to optimize the density matrix. However, for systems such as $Y_2Mo_2O_7$ in which GGA results in a (wrong) metallic state, it is possible to have multiple minima due to degrees of freedom in the density-matrix occupation. These degrees of freedom in the density matrix happen because of partially occupied d -orbital states at the Fermi level. It is also worth mentioning that the density-matrix occupations are under the influence of symmetry. Higher symmetry lowers the degrees of freedom in the density matrix and, in some cases such as $Y_2Mo_2O_7$, restricts GGA+ U calculations to some incorrect solutions.

To explore the possibilities in density-matrix occupation for $Y_2Mo_2O_7$, we manipulate the initial density-matrix occupations of Mo atoms at the starting point of GGA+ U calculations with symmetry breaking for the antiferromagnetic configuration. We use $U_{eff} = 3.5$ eV to correct on-site electron-electron Coulomb repulsion on $4d$ orbitals in $Y_2Mo_2O_7$ [10]. For our exploration of density-matrix occupation, we consider 150 different initial density-matrix occupations. These initial density-matrix occupations lead to 50 distinguishable electronic configurations as the result of GGA+ U self-consistent field calculations. Figure 6 shows the total energy of these 50 GGA+ U solutions versus their density matrix occupations, which is represented by a number (from 1 to 50). Among these 50 GGA+ U solutions, we focus on insulating ones. Despite differences in density-matrix occupations, the insulating GGA+ U solutions are nearly degenerate in terms of energy. To characterize the difference between these nearly degenerate states, we select two of them (the ones denoted by arrows in Fig. 6) and compare their d -orbital orientations at the tetrahedron corners. Figure 7 shows that despite the same spin magnetic moment directions, there are tiny differences in the orbital orientations of these two electronic configurations. These orbital degrees of freedom create local distortions and cause the system to show spin-glass behavior [10,37]. In contrast, for $Y_2Mn_2O_7$, we reach a single solution where orbital orientations at the tetrahedron corners show a single direction.

IV. CONCLUSIONS

In this paper, we tried to shed light on the magnetic state of the pyrochlore $Y_2Mn_2O_7$ using *ab initio* GGA+ U

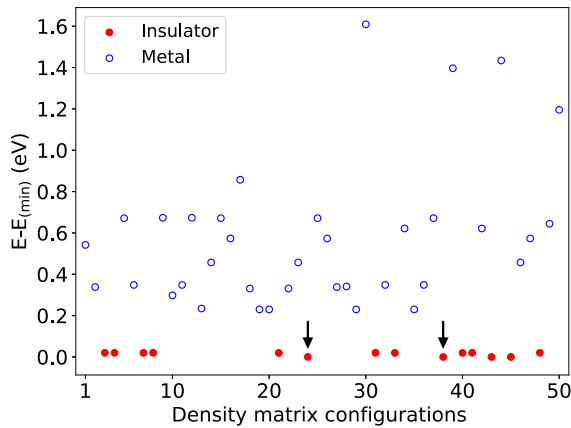


FIG. 6. Total energy of $Y_2Mo_2O_7$ versus density matrix occupations. The x axis representatively indicates different density matrix occupations. We set the minimum of total energy to zero. The solid red and open blue circles indicate insulator and metallic solutions, respectively. The black arrows show two insulator solutions that we select as instances to examine d -orbital orientation.

calculations and Monte Carlo simulations. For GGA+ U calculations, we estimated Hubbard U_{eff} via the linear-response method. Using GGA+ U calculations, we constructed several spin models for $Y_2Mn_2O_7$ by tuning the Hubbard parameter U_{eff} around its estimated value. By comparing Monte Carlo simulations of these models with experimental measurements such as the Curie-Weiss temperature, we found that the ferromagnetic state of $Y_2Mn_2O_7$ almost matches the experiments. Also, we proved that $Y_2Mn_2O_7$ cannot have a d -orbital degree of freedom mechanism which may turn $Y_2Mn_2O_7$ into a

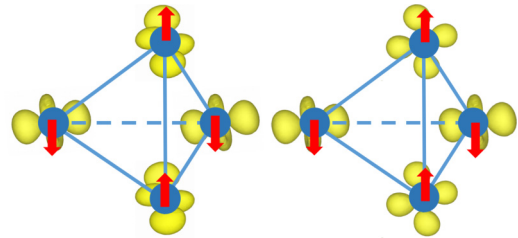


FIG. 7. The orbital orientation of the $4d$ band nearly below the Fermi level for two approximately degenerate GGA+ U solutions for $Y_2Mo_2O_7$.

spin-glass system. To examine this issue, we analyzed both $Y_2Mn_2O_7$ and $Y_2Mo_2O_7$, where for the latter, there is evidence of spin-glass behavior due to the d -orbital degree of freedom mechanism. We demonstrated that while GGA+ U calculations reveal the d -orbital degree of freedom mechanism in $Y_2Mo_2O_7$, there is no way that GGA+ U leads to such machinery for $Y_2Mn_2O_7$. In summary, we suggest that a pure pyrochlore phase of $Y_2Mn_2O_7$ is a simple ferromagnetic system. We also propose further experiments on this material to clarify this issue. As a general outline, given the availability of modern laboratory equipment, the results of the neutron scattering measurements can be repeated once again, and the absence or presence of a sharp Bragg peak can be reexamined.

ACKNOWLEDGMENTS

M. Amirabbasi thanks M. Ležaić, G. Bihlmayer, and F. Shabazi for useful discussions. The authors thank N. Rezaei for her constructive comments.

- [1] C. Lacroix, P. Mendels, and F. Mila, *Introduction to Frustrated Magnetism*, Springer Series in Solid-State Science (Springer, Heidelberg, 2011).
- [2] J. E. Greedan, *J. Mater. Chem* **11**, 37 (2001).
- [3] J. S. Gardner, M. J. P. Gingras, and J. E. Greedan, *Rev. Mod. Phys.* **82**, 53 (2010).
- [4] L. Savary and L. Balents, *Phys. Rev. Lett.* **118**, 087203 (2017).
- [5] J. Gaudet, E. M. Smith, J. Dudemaine, J. Beare, C. R. C. Buhariwalla, N. P. Butch, M. B. Stone, A. I. Kolesnikov, G. Xu, D. R. Yahne, K. A. Ross, C. A. Marjerrison, J. D. Garrett, G. M. Luke, A. D. Bianchi, and B. D. Gaulin, *Phys. Rev. Lett.* **122**, 187201 (2019).
- [6] L. Balents, *Nature (London)* **464**, 199 (2010).
- [7] N. R. Davies, C. V. Topping, H. Jacobsen, A. J. Princep, F. K. K. Kirschner, M. C. Rahn, M. Bristow, J. G. Vale, I. da Silva, P. J. Baker, C. J. Sahle, Y.-F. Guo, D.-Y. Yan, Y.-G. Shi, S. J. Blundell, D. F. McMorrow, and A. T. Boothroyd, *Phys. Rev. B* **99**, 174442 (2019).
- [8] D. K. Singh and Y. S. Lee, *Phys. Rev. Lett.* **109**, 247201 (2012).
- [9] H. Kawamura and T. Taniguchi, *Handbook of Magnetic Materials*, edited by K. H. J. Buschow (Elsevier, 2015), pp. 1–137.
- [10] H. J. Silverstein, K. Fritsch, F. Flicker, A. M. Hallas, J. S. Gardner, Y. Qiu, G. Ehlers, A. T. Savici, Z. Yamani, K. A. Ross, B. D. Gaulin, M. J. P. Gingras, J. A. M. Paddison, K. Foyevtsova, R. Valenti, F. Hawthorne, C. R. Wiebe, and H. D. Zhou, *Phys. Rev. B* **89**, 054433 (2014).
- [11] N. P. Raju, E. Gmelin, and R. K. Kremer, *Phys. Rev. B* **46**, 5405 (1992).
- [12] M. J. P. Gingras, C. V. Stager, N. P. Raju, B. D. Gaulin, and J. E. Greedan, *Phys. Rev. Lett.* **78**, 947 (1997).
- [13] O. Ofer, A. Keren, J. S. Gardner, Y. Ren, and W. A. MacFarlane, *Phys. Rev. B* **82**, 092403 (2010).
- [14] J. E. Greedan, D. Gout, A. D. Lozano-Gorrin, S. Derahkshan, T. Proffen, H.-J. Kim, E. Božin, and S. J. L. Billinge, *Phys. Rev. B* **79**, 014427 (2009).
- [15] J. N. Reimers, J. E. Greedan, R. K. Kremer, E. Gmelin, and M. A. Subramanian, *Phys. Rev. B* **43**, 3387 (1991).
- [16] B. D. Gaulin, J. N. Reimers, T. E. Mason, J. E. Greedan, and Z. Tun, *Phys. Rev. Lett.* **69**, 3244 (1992).
- [17] H. Zhou, C. Wiebe, J. Janik, B. Vogt, A. Harter, N. Dalal, and J. Gardner, *J. Solid State Chem.* **183**, 890 (2010).
- [18] Y. Shimakawa, Y. Kubo, N. Hamada, J. D. Jorgensen, Z. Hu, S. Short, M. Nohara, and H. Takagi, *Phys. Rev. B* **59**, 1249 (1999).
- [19] M. Subramanian, C. Torardi, D. Johnson, J. Pannetier, and A. Sleight, *J. Solid State Chem.* **72**, 24 (1988).
- [20] J. Reimers, J. Greedan, and M. Sato, *J. Solid State Chem.* **72**, 390 (1988).

- [21] FLEURgroup, FLEUR, <http://www.flapw.de/>.
- [22] P. Giannozzi, S. Baroni, N. Bonini, M. Calandra, R. Car, C. Cavazzoni, D. Ceresoli, G. L. Chiarotti, M. Cococcioni, I. Dabo, A. D. Corso, S. de Gironcoli, S. Fabris, G. Fratesi, R. Gebauer, U. Gerstmann, C. Gougousis, A. Kokalj, M. Lazzeri, L. Martin-Samos, N. Marzari, F. Mauri, R. Mazzarello, S. Paolini, A. Pasquarello, L. Paulatto, C. Sbraccia, S. Scandolo, G. Sclauzero, A. P. Seitsonen, A. Smogunov, P. Umari, and R. M. Wentzcovitch, *J. Phys.: Condens. Matter* **21**, 395502 (2009).
- [23] K. F. Garrity, J. W. Bennett, K. M. Rabe, and D. Vanderbilt, *Comput. Mater. Sci.* **81**, 446 (2014).
- [24] J. P. Perdew, K. Burke, and M. Ernzerhof, *Phys. Rev. Lett.* **77**, 3865 (1996).
- [25] A. O. de-la Roza, E. R. Johnson, and V. Luaña, *Comput. Phys. Commun.* **185**, 1007 (2014).
- [26] A. O. de-la Roza, M. Blanco, A. M. Pendás, and V. Luaña, *Comput. Phys. Commun.* **180**, 157 (2009).
- [27] V. I. Anisimov, J. Zaanen, and O. K. Andersen, *Phys. Rev. B* **44**, 943 (1991).
- [28] L. Vaugier, H. Jiang, and S. Biermann, *Phys. Rev. B* **86**, 165105 (2012).
- [29] M. Cococcioni and S. de Gironcoli, *Phys. Rev. B* **71**, 035105 (2005).
- [30] H. J. Kulik, M. Cococcioni, D. A. Scherlis, and N. Marzari, *Phys. Rev. Lett.* **97**, 103001 (2006).
- [31] A. Sadeghi, M. Alaei, F. Shahbazi, and M. J. P. Gingras, *Phys. Rev. B* **91**, 140407(R) (2015).
- [32] T. Moriya, *Phys. Rev.* **120**, 91 (1960).
- [33] K. Hukushima and K. Nemoto, *J. Phys. Soc. Jpn.* **65**, 1604 (1996).
- [34] N. Rezaei, M. Alaei, and H. Akbarzadeh, [arXiv:1912.00793](https://arxiv.org/abs/1912.00793).
- [35] M. Elhajal, B. Canals, R. Sunyer, and C. Lacroix, *Phys. Rev. B* **71**, 094420 (2005).
- [36] C. Donnerer, M. C. Rahn, M. M. Sala, J. G. Vale, D. Pincini, J. Stremper, M. Krisch, D. Prabhakaran, A. T. Boothroyd, and D. F. McMorrow, *Phys. Rev. Lett.* **117**, 037201 (2016).
- [37] H. Shinaoka, Y. Motome, T. Miyake, and S. Ishibashi, *Phys. Rev. B* **88**, 174422 (2013).
- [38] M. Subramanian, G. Aravamudan, and G. S. Rao, *Mater. Res. Bull.* **15**, 1401 (1980).
- [39] B. Meredig, A. Thompson, H. A. Hansen, C. Wolverton, and A. van de Walle, *Phys. Rev. B* **82**, 195128 (2010).
- [40] N. Deilynazar, E. Khorasani, M. Alaei, and S. J. Hashemifar, *J. Magn. Magn. Mater.* **393**, 127 (2015).